Research Square

Preprints are preliminary reports that have not undergone peer review.
They should not be considered conclusive, used to inform clinical practice,
or referenced by the media as validated information.

An ITO@AgNWs enhanced electrochemical biosensor for rapid quantitative detection of sweet substances

Wuzhen Qi
Beijing University of Chinese Medicine
Minhao Niu
Ningxia University
Zihan Xue
Beijing University of Chinese Medicine
Yayuan Li
Beijing University of Chinese Medicine
Xuanqi Ke
Beijing University of Chinese Medicine
Yue Liu
Beijing University of Chinese Medicine
Zhishu Tang
Beijing University of Chinese Medicine
Bing Xu
xubing@bucm.edu.cn

Beijing University of Chinese Medicine

Research Article

Keywords: silver nanowires, electrochemistry, biosensing, detection device, T1R2 receptor, sweet substances

Posted Date: October 23rd, 2026

DOI: https://doi.org/10.21203/rs.3.rs-11111661/v1

License: This work is licensed under a Creative Commons Attribution 4.0 International License.
Read Full License

Additional Declarations: No competing interests reported.

Abstract

Quantitative evaluation of flavor compounds is essential for effective flavor masking and taste modulation, and underpins the consistent quality of both food and pharmaceutical products. In this study, an electrochemical biosensor based on taste receptors and silver nanowires signal amplification was successfully constructed for the rapid quantitative detection of taste substances in complex components. Atractylenolide I (ATR-I) was employed as a model sweet-tasting compound. The type 1 taste receptor member 2 (T1R2) specifically bound ATR-I when immobilized on a silver nanowires (AgNWs) modified ITO electrode, enabling the conversion of ATR-I concentration into electrochemical signals. The modification of the ITO electrode with AgNWs significantly enhanced its sensing sensitivity while simultaneously providing high-affinity binding sites for protein immobilization. The results indicate that the proposed biosensor was capable of detecting ATR-I as low as 1.8×10^{-13} mol/L from a complex drug background within 20 min, with a linear detection range of 10^{-11} mol/L to 10^{-6} mol/L. Moreover, this biosensor exhibits high reproducibility, stability, sensitivity, and practicality, offering a novel approach for the quantitative detection of sweeteners in complex matrices.

Introduction

Glucose, sucrose, and other sugars elicit a distinct sweet taste sensation in humans[1]. In dietary contexts, excessive consumption of sweet substances—often highly preferred—can contribute to the development of diabetes and obesity[2]. Among Chinese materia medica, sweet-tasting herbs such as Atractylodes are commonly associated with functions including nourishing the body, alleviating pain, and regulating spleen and stomach functions[3]. Therefore, the quantitative analysis of sweet substances is highly significant for disease prevention—particularly diabetes—as well as for elucidating drug efficacy mechanisms, evaluating drug quality, and improving pharmaceutical taste. Traditional methods for the quantitative detection of sweet substances, such as electronic nose, electronic tongue, and high-performance liquid chromatography (HPLC)[4, 5], offer high sensitivity but require sophisticated and expensive equipment, depend on skilled laboratory personnel, and entail high operational costs. Therefore, it is highly significant to develop a simple, rapid, and sensitive method for the detection of sweet substances[6].

Type 1 Taste Receptor Member 2 (T1R2) is a key bioreceptor involved in mammalian sweet taste perception and belongs to the G protein-coupled receptor (GPCR) family. It has been reported[7] that it is capable of binding to a wide variety of sweet-tasting substances, including natural sugars (glucose, fructose), artificial sweeteners (aspartame, saccharin), and sweetness proteins (Brazilian sweeteners)[8–10], in order to mediate sweetness signal transduction[11, 12]. Compared to traditional taste detection methods (e.g., animal behavioural methods), T1R2 is an ideal target for the development of modern taste biosensors due to its high ligand compatibility, well-defined signaling cascade pathways, and tissue distribution specificity.

Electrochemical biosensors have drawn significant attention in the field of analysis owing to their rapid response, high sensitivity, and high selectivity[13–15]. Indium tin oxide (ITO) electrode, a high-performance transparent conductive oxide (TCO) material, possesses excellent combined electrical and optical properties, which offers an ideal platform for electrochemical signal transduction and optical real-time monitoring[16]. In the field of biosensing, the ease of surface modification of ITO electrodes is a key advantage, enabling the efficient immobilization of biorecognition elements through chemical groups (e.g., carboxyl groups, amino groups) or nanomaterial composites. For example, amphiphilic ion-pair modifications on ITO surfaces (e.g., $-SO_3^-/N^+(Me)_3$ antifouling groups combined with $COOH/NH_2$ linkers) enhance protein immobilization efficiency and significantly improve anti-fouling performance in complex matrices[17]. In addition, ITO substrates have been successfully applied in taste receptor integration, and their conductivity enables sensitive conversion of receptor-ligand binding events into electrochemical signals, providing a stable and low-cost platform for the detection of sweet taste substances[18, 19].

Atractylenolide I (ATR-I), a bioactive sesquiterpene lactone isolated from the dried rhizome of Atractylodes macrocephala, is a key pharmacologically active compound with significant anti-inflammatory, antitumor, and gastrointestinal regulatory effects. It is also a major constituent responsible for the spleen-strengthening properties of Atractylodes macrocephala. Studies have demonstrated that ATR-I possesses sweet taste characteristics[20, 21].

In this study, a novel electrochemical biosensor enhanced by AgNWs has been developed for the rapid, highly sensitive, and low-cost detection of sweet substances in pharmaceuticals. ATR-I was used as a representative sweet-taste compound. AgNWs were first synthesized via the polyol method and then immobilized on the surface of the ITO electrode through a solvent impregnation and thermal melting process[22, 23]. Subsequently, the T1R2 receptor was employed as the sensitive recognition element for sweet substances and immobilized on the AgNWs surface via mercaptopropionic acid. The ATR-I in the sample is adsorbed onto the electrode surface via interaction with the T1R2 receptor, leading to a change in electrical signal, which is then used to quantify the ATR-I content in the sample by differential pulse voltammetry (DPV).

Experimental

Reagents and instruments

Silver nitrate was purchased from Beijing Tongguang Fine Chemical Company (Beijing, China); ethylene glycol ($C_2H_6O_2$) from Tianjin Zhiyuan Chemical Reagent Company (Tianjin, China); ferric chloride hexahydrate ($FeCl_3 \cdot 6H_2O$) from Fuchen Chemical Reagent Company (Tianjin, China); and polyvinylpyrrolidone (PVP) from Shanghai McLean Biochemistry and Technology Company (Shanghai, China). N-hydroxysuccinimide (NHS) and 1-(3-dimethylaminopropyl)-3-ethylcarbodiimide (EDC) were obtained from Sigma-Aldrich (Shanghai, China). 3-Mercaptopropionic acid (MPA) was purchased from Beijing Zhongnong Boshi Technology Co. (Beijing, China). Glucose, atractylenolide I, ferulic acid,

capsaicin, and amygdalin were purchased from Shanghai Shidande Technology (Shanghai, China). T1R2 protein was acquired from CUSABIO Technology LLC (Wuhan, China). According to the manufacturer's documentation, the protein comprised amino acids 20–839 of human T1R2, contained an N-terminal 10×His tag, and was produced using an in vitro *E. coli*-based expression system. Its predicted molecular weight was 99.1 kDa, and its purity was ≥ 85%, as determined by SDS–PAGE.

All electrochemical measurements were performed using a CHI660E electrochemical workstation (Shanghai Chenhua Instrument Co., Ltd., China). The reactor was supplied by Xi'an Chang Yi Instrument Company (Xi'an, China), the electric constant-temperature blast drying oven by Shanghai Qixin Scientific Instrument Company (Shanghai, China), the ultrasonic cleaner by Kunshan Ultrasonic Instrument Co., Ltd. (Kunshan, China), and the electronic analytical balance by Sartorius Scientific Instruments (Beijing, China). Electronic tongue measurements were conducted using an SA402B electronic tongue system (INSENT Inc., Japan).

Preparation of AgNWs

AgNWs were synthesized using a modified polyol method[24]. Briefly, 200 mg of PVP was first dissolved in 25 mL of ethylene glycol, followed by the addition of 300 mg of silver nitrate to the resulting solution. After stirring until the solution became clear, it was wrapped in tinfoil and sonicated for 5 min to ensure complete dissolution. Subsequently, $FeCl_3 \cdot 6H_2O$ was dissolved in ethylene glycol to prepare a 650 μmol/L solution, and 3 mL of this solution was added to the PVP and silver nitrate mixture. Finally, the mixture was transferred to the polytetrafluoroethylene liner of a 50 mL stainless steel autoclave and heated at 140°C for 6 h. After cooling to room temperature, the AgNWs were collected by centrifugation and washed three times with acetone and ethanol. The resulting AgNWs dispersion in ethanol was stored at room temperature for subsequent use.

Preparation of ITO electrodes

ITO electrodes were prepared using the impregnation method with minor modifications. Briefly, the ITO electrode was cleaned sequentially with deionized water, isopropanol, and acetone. Subsequently, the AgNWs were sonicated for 5 min to disperse aggregates, and the resulting homogeneous solution was added dropwise to the detection area of the ITO electrode (10 mm in diameter). The electrode was then dried at 25°C for 5 min and further heated at 200°C for 2 h to fuse the junctions between the AgNWs.

Construction of biosensors

First, 60 μL of mercaptopropionic acid (3-MPA) was added dropwise to the AgNW-modified ITO electrode and incubated at 25°C for 17–24 h. Then, after washing with deionised water, 30 μL of a mixed solution of NHS and EDC was added and incubated at room temperature for 15 min to activate the carboxyl groups on the AgNWs. After removal of the mixed solution, the electrode was rinsed twice with 60 μL of

phosphate-buffered saline (PBS). Finally, 30 μL of T1R2 receptor protein solution (0.1 mg/mL) was added and incubated at 4°C for 2 h, followed by storage at 4°C for future use.

Electrochemical detection

To investigate the stepwise fabrication process of the working electrode, differential pulse voltammetry (DPV) measurements were performed sequentially in a solution containing 10 mM potassium ferricyanide and 0.1 M potassium chloride. The DPV measurements were conducted at a scan rate of 0.04 V/s, over a potential range from − 0.4 V to 0.6 V, with a sampling interval of 0.004 V and a signal sensitivity of 1×10^{-4} A/V. The response signals (current values) corresponding to before and after the binding of T1R2 to sweet substances were collected. Pure water was used as the blank control. The normalized current change rate(*CR*) was calculated according to the following formula.

$$\mathrm{CR}=\frac{\mathrm{I_{blank}}\text{-}\mathrm{I_{bind}}}{\mathrm{I_{blank}}}\#(1)$$

where $\mathbf{I}_{blank}$ represents the current value of the blank group, and $\mathbf{I}_{bind}$ represents the current value after T1R2 binds to sweet substances.

Results and discussion

Detection principle

AgNWs were immobilized on a clean ITO surface through impregnation and subsequent heat treatment to form a uniform conductive network. Due to the high conductivity of AgNWs, this hierarchical network facilitates electron transfer, significantly reducing internal resistance during electrochemical detection and amplifying the detection signal, thus making it an ideal nanomaterial for immobilizing proteins such as T1R2. 3-MPA was immobilized on the surface of AgNWs via silver–sulfur bonding. Following activation with EDC and NHS, 3-MPA enabled the covalent attachment of T1R2 to the AgNWs through peptide bond formation. The immobilized T1R2 can effectively bind sweet target molecules. The binding event raises the interfacial barrier on the electrode surface and hinders electron transfer of redox probes. This weakened electron transport efficiency ultimately leads to a decline in DPV peak current, and the magnitude of current reduction correlates positively with the quantity of captured sweet analytes. Differential pulse voltammetry (DPV) was further applied to quantify the relationship between signal attenuation and the concentration of sweet substances.

Material characterisation

AgNWs play a crucial role in enhancing the sensitivity of the biosensor. In this study, the synthesis of AgNWs was characterized by X-ray diffraction (XRD), scanning electron microscopy (SEM), transmission electron microscopy (TEM), and X-ray photoelectron spectroscopy (XPS), with results presented in Fig. 1.

The XRD results in Fig. 1a show that the diffraction peaks of the AgNWs at 2θ = 38.13° and 44.67° correspond to the (100) and (111) crystal planes of silver with a face-centered cubic structure, respectively. SEM (Fig. 1b) and TEM (Fig. 1c) reveal that the synthesized AgNWs are uniform in size and shape (approximately 20 μm in length and 150 nm in diameter) and well dispersed. Meanwhile, the XPS results revealed distinct characteristic peaks of Ag 3D, and the levels of non-target elements such as C and O were below the detection limit, indicating a clean surface of the synthesized AgNWs free from impurity adsorption. This comprehensive characterization demonstrates that the synthesized AgNWs meet high-quality standards in terms of structural integrity, chemical purity, and morphological controllability.

Step-by-step modification of electrodes

As shown in Fig. 2a, SEM revealed that the surface of the bare glass sheet was very smooth. However, it appeared wrinkled after ITO modification (Fig. 2b), providing a suitable substrate for AgNWs attachment. In addition, SEM showed that the AgNWs were firmly bonded to the ITO surface (Fig. 2c). Figure 2e and 3f show the ITO electrode modified with AgNWs and the packaged microfluidic chip, respectively. Figure 2g presents the XPS characterization of the ITO electrode after protein modification, showing the elemental composition of carbon, phosphorus, sulfur, silver, indium, tin, and oxygen. Among these, the presence of silver plays a key role in the construction of high-performance electrochemical sensing interfaces. Compared with conventional noble metals such as gold (Au), platinum (Pt), and palladium (Pd), silver has become a widely used substrate modification material in electrochemical sensors due to its prominent advantages of high crustal abundance and low cost[25–28]. Figure 2d shows the gradual changes in current during the differential pulse voltammetry measurement throughout the modification process. The bare ITO electrode exhibits a weak electrical signal, which is significantly enhanced after AgNWs modification due to their high conductivity. This enhancement is attributed to the structural characteristics of the silver nanowires, which facilitate electron transfer at the electrode–analyte interface, thereby improving the detection sensitivity of the electrochemical sensor[29]. The addition of 3-MPA led to the formation of a self-assembled monolayer via silver–sulfur bonding on the surface of AgNWs, resulting in a reduced electrical signal.

After the T1R2 protein was modified, the electrical signals decreased significantly compared to the 3-MPA modified device, indicating that the successful modification of the protein impeded the transfer of electrons at the electrode surface. Finally, upon injection of glucose solution into the biosensor, the electrical signal further decreased due to glucose trapping by the T1R2 protein.

Optimisation of experimental conditions

To achieve optimal detection performance of the biosensor, key experimental parameters were systematically optimized in this study, including the amount of AgNWs, the concentration and modification time of T1R2 receptor protein, and the capture time. The parameter optimization process was based on a one-factor-at-a-time experimental design, with real-time monitoring of current changes

on the electrode surface using the DPV method. Pure water was set as the blank control group, and 10 nM ATR-I solution served as the positive experimental group.The optimal parameter combinations were determined by evaluating the relative change in sensor current change rate(CR) under different conditions. All experiments were performed in triplicate under identical conditions to ensure data reliability.

As shown in Fig. 3a, the current increased as the volume of AgNWs used for modification increased from 10 μL to 60 μL. At low AgNW loadings, an incomplete conductive network with abundant gaps was formed on the electrode surface, which limited the available pathways and hindered electron-transfer kinetics. As the dosage increased, overlapping AgNWs constructed a continuous interconnected network, providing sufficient channels to facilitate electron transport and thus resulting in a remarkable enhancement of current response. The normalized electrical signals *CR* in Fig. 3b indicate that the conductivity and electrochemical activity of the electrode are optimal when the volume of AgNWs is 30 μL. As the AgNWs loading on the electrode increases, the current monotonically rises; however, the *CR* elicited by analyte binding progressively diminishes. This phenomenon may be attributed to an excessively high absolute base current, which obscuring the specific electrochemical signature arising from target-receptor binding. Therefore, 30 μL was selected as the optimal modification volume of AgNWs.

Figure 3c and Fig. 3d demonstrate the effect of T1R2 protein dosage on the biosensor properties. As the T1R2 dosage increased from 1 μg to 4 μg, the electrode current exhibited a decreasing trend, attributable to the formation of a protein layer that blocks the electron transfer pathway and increases charge transfer resistance. A further increase in protein dosage from 4 μg to 6 μg resulted in no significant change in CR, indicating that a dense protein layer had been fully formed on the electrode surface at this stage. Therefore, the T1R2 dosage was optimized to 4 μg.

Figure 3e and Fig. 3f demonstrate the effect of different protein modification durations on the biosensor properties. The results show that as the modification time increased from 0.5 h to 2.0 h, the rate of current change gradually increased, indicating that the amount of protein bound to the AgNWs increased with prolonged incubation time. When the protein modification time was further increased from 2.0 h to 3.0 h, no significant change in current was observed, indicating that sufficient protein had been bound to the electrode surface by this time. Therefore, the optimal modification time for the T1R2 receptor in the biosensor was determined to be 2.0 h.

Figure 3g and Fig. 3h demonstrate the effect of reaction time on the biosensor. As the capture time increased from 5 min to 20 min, both the peak current value and the rate of current change increased significantly, indicating progressive binding of ATR-I by the T1R2 receptor. The bound ATR-I formed an additional insulating layer on the electrode surface, leading to a rapid increase in the charge transfer resistance, which in turn reduced the current significantly. When the reaction time was further increased from 20 min to 30 min, no significant change in current was observed, indicating that the binding rate of the T1R2 receptor to ATR-I had reached a dynamic equilibrium with the dissociation rate, and the net

amount of bound analyte no longer increased. Therefore, 20 min was selected as the optimal reaction time for sample analysis.

Sensor analysis performance validation

The performance of the proposed biosensor was evaluated by measuring different concentrations of ATR-I standards (10^{-14}-10^{-5} mol/L) under optimal experimental conditions. As shown in Fig. 4a, within the range of 10^{-11} to 10^{-6} mol/L, the peak current signal of the DPV response decreased from 1.91×10^{-4} to 1.32×10^{-4} as the concentration of ATR-I increased, and the CR increased from 0.13 to 0.4 The corresponding regression equation was $CR = 0.0544\log C + 0.7224$ ($R^2 = 0.9962$). Based on the $3\sigma/k$ criterion, where σ (0.00968) represents the standard deviation of blank measurements and k (0.0544) is the absolute slope of the calibration curve, the limit of detection (LOD) of this biosensor was calculated to be 1.8×10^{-13} mol/L.

The excellent performance can be attributed to the following aspects: 1) AgNWs modified on the surface of the ITO electrode form an efficient conductive network. The high conductivity and large specific surface area of AgNWs not only significantly reduce charge transfer resistance at the electrode interface and enhance electron transfer efficiency, but also increase surface loading capacity through three-dimensional nanostructures, providing abundant binding sites for subsequent immobilization of receptor proteins. 2) As a natural receptor for sweet molecules, T1R2 exhibits high affinity and selectivity toward sweet targets such as ATR-I. 3) Optimisation of protein modification amount and modification time ensures the formation of a compact, activity-retaining protein layer on the electrode surface, thereby enhancing binding efficiency and signal stability. 4) The physical adsorption of AgNWs combined with protein immobilization techniques (e.g., chemical cross-linking) reduces the risk of interfacial molecule detachment, while optimization of the capture time ensures complete binding of target molecules during the dynamic equilibrium phase and prevents protein inactivation or dissociation caused by over-incubation. This multilayer process optimization enables the sensor to maintain reliable detection performance in complex sample matrices.

Examination of specificity

The treated ATR-I, glucose, ferulic acid, capsaicin, and bitter amygdalin were selected for molecular docking with the binding site region of the T1R2 protein to elucidate the specificity of the T1R2 protein and the key role of sweetness as a taste attribute of ATR-I from the perspective of molecular simulation. The detailed procedures and conditions of the molecular docking simulation are described in the supplementary materials. The molecular docking scores are presented in Table 1. From the molecular docking results and mechanistic analysis, the T1R2 receptor exhibits high selectivity and specificity toward ATR-I. The molecular docking score of ATR-I was as high as 92.4245, significantly higher than those of glucose (88.2195) and Capsaicin (71.3126), indicating its strong binding affinity and stable interaction with T1R2.

Table 1
Scores of molecular docking

Sample	CAS	Docking Score
ATR-I	73069-14-4	92.4245
Glucose	58367-01-4	88.2195
Ferulic Acid	1135-24-6	62.3304
Capsaicin	2444-46-4	71.3126
Bitter Amygdalin	29883-15-6	58.8144

As shown in Fig. 5, ATR-I primarily forms hydrophobic interactions with the surrounding LEU residues, as well as van der Waals forces, hydrogen bonding, and other interactions with PHE, HIS, and ASN, thereby forming a more stable complex. To further analyze the types of interactions between the T1R2 protein and ligand molecules, a two-dimensional schematic diagram of the interactions is presented in Fig. 5a, enabling more intuitive visualization of the intermolecular interactions as well as the key amino acid residues and functional motifs involved.

Using the proposed biosensor to detect these five samples at an identical concentration of 1×10^{-4} mol/L, as shown in Fig. 5c, the current response triggered by ATR-I is significantly higher than that induced by the other molecules, which is consistent with the molecular docking results and fully demonstrates that the biosensor can accurately identify and specifically respond to ATR-I.

To further verify the sweet-taste characteristic of ATR-I and validate the above mechanism, electronic tongue detection was performed with sucrose serving as the sweetness reference. The results showed that 200 μmol/L ATR-I produced a prominent response signal in the sweetness sensing channel, which objectively confirmed the sweet-taste property of ATR-I and further verified its specific binding capability with the T1R2 receptor. Full experimental details and related data are provided in the Supplementary Materials.

Reproducibility and stability

To verify the reproducibility and stabilitythis of this biosensor, the intra-batch and inter-batch reproducibility as well as long-term storage stability of the sensor were systematically evaluated. As shown in Fig. 6a and Fig. 6b, inter-batch reproducibility was assessed using sensors from six independent batches, with three chips tested in each batch. The measured signal-change amplitudes spanned 2.14×10^{-4}–2.45×10^{-4} A, with a signal fluctuation reaching approximately 14.49%. Slight inter-batch variation was observed. This minor discrepancy is most likely introduced by manual electrode-fabrication operations rather than inherent flaws of the modification strategy itself. Overall, satisfactory inter-batch consistency of the fabrication strategy was still achieved. For intra-batch reproducibility, six biosensor chips fabricated within the same batch delivered highly consistent DPV signals (Fig. 6c and

6d). The peak-current-derived signal-change ratios of these six electrodes ranged narrowly from 2.19×10^{-4} to 2.25×10^{-4} A, with a maximum signal fluctuation of only 2.74%. This demonstrates favorable intra-batch precision, which is primarily attributed to the standardized modification process with precise dosage control of modification materials.

To further characterize the long-term storage stability of the biosensors, freshly prepared electrodes were sealed and stored in a refrigerator at 4°C. At scheduled time-points (day 1, 3, 5, 7, 9, 11 and 13), sensors were taken out from storage, followed by incubation with ATR-I solution at a fixed concentration of 1 nM. DPV measurements were then performed under identical experimental conditions to record the electrochemical response at each time interval. As shown in Fig. 6e and 6f, the relative current changes remained relatively stable within 7 days of storage, indicating that biosensor performance could be well preserved. Nevertheless, obvious signal fluctuation occurred after 9-day storage, which was most likely caused by the inactivation of surface-immobilized proteins. Collectively, these results reveal that the biosensor maintains reliable sensing performance toward ATR-I within 7 days after preparation, and all detection assays should be completed within this valid storage period.

To further evaluate the practical applicability of the developed biosensor, ATR-I in real Atractylodes macrocephala samples was quantified by both the proposed biosensor and liquid chromatography-mass spectrometry (LC-MS) method. The corresponding quantitative results and comparative analysis are provided in the Supplementary Materials.

A comprehensive performance comparison between the developed biosensor and other similar reported sensors has been presented in the supplementary materials, which further demonstrates the superiorities of the proposed sensor in detection efficiency, sensitivity and detection range.

Conclusions

In this study, a novel biosensor was successfully developed for the rapid and sensitive evaluation of sweet substances for Chinese materia medica. AgNWs were employed to modify ITO electrodes, providing binding sites for receptor proteins and enhancing the biosensor's sensitivity. The T1R2 glycoprotein was utilizedas a receptor for sweet substances to enable specific recognition and capture. Microfluidic chips provide a low-sample-consumption and highly efficient reaction environment. Under optimized conditions, the proposed biosensor can quantify the content of sweet substances in samples within 20 min, with a linear detection range of 10^{-11} to 10^{-6} mol/L and a limit of detection (LOD) of 1.8×10^{-13} mol/L. This biosensor has the potential to extend from rapid quantitative analysis of sweet substances to other flavor compounds, providing a scientific basis for theoretical research on the property theory of Chinese materia medica and for quality control in food applications.

Declarations

AI disclosure

AI-assisted technology is not used in the preparation of this manuscript (except checking grammar and spelling).

CRediT authorship contribution statement

Wuzhen Qi: Conceptualization, Funding acquisition, Methodology, Writing – review & editing. **Minhao Niu**: Writing – original draft, Methodology, Visualization, Validation. Data curation. **Zihan Xue**: Writing – original draft, Methodology, Data curation. **Yayuan Li**: Writing – review & editing, Data curation, Resources. **Xuanqi Ke**: Writing – review & editing, Resources. **Yue Liu**: Investigation, Methodology, Writing – review & editing. **Zhishu Tang**: Funding acquisition, Resources, Supervision, Writing – review & editing. **Bing Xu**: Conceptualization, Funding acquisition, Validation, Writing – review & editing.

Funding

This work was supported by the National Natural Science Foundation of China (No. 82304720), the National Major Scientific and Technological Projects for New Drug Development (No. 2025ZD1801004) and the Fundamental and Interdisciplinary Disciplines Breakthrough Plan of the Ministry of Education of China (No. JYB2025XDXM612).

Declaration of Competing Interest

The authors declare no conflict of interest.

References

1. Liu, W. W.; Bohorquez, D. V. The neural basis of sugar preference. Nat Rev Neurosci **2022**, *23* (10), 584-595. DOI: 10.1038/s41583-022-00613-5
2. Te Morenga, L. A.; Howatson, A. J.; Jones, R. M.; Mann, J. Dietary sugars and cardiometabolic risk: systematic review and meta-analyses of randomized controlled trials of the effects on blood pressure and lipids. Am J Clin Nutr **2014**, *100* (1), 65-79. DOI: 10.3945/ajcn.113.081521
3. Heo, G.; Kim, Y.; Kim, E. L.; Park, S.; Rhee, S. H.; Jung, J. H.; Im, E. Atractylodin Ameliorates Colitis via PPARalpha Agonism. Int J Mol Sci **2023**, *24* (1). DOI: 10.3390/ijms24010802
4. Jalaludin, I.; Kim, J. Comparison of ultraviolet and refractive index detections in the HPLC analysis of sugars. Food Chem **2021**, *365*, 130514. DOI: 10.1016/j.foodchem.2021.13051
5. Qin, C.; Qin, Z.; Zhao, D.; Pan, Y.; Zhuang, L.; Wan, H.; Di Pizio, A.; Malach, E.; Niv, M. Y.; Huang, L.; et al. A bioinspired in vitro bioelectronic tongue with human T2R38 receptor for high-specificity detection of N-C=S-containing compounds. Talanta **2019**, *199*, 131-139. DOI: 10.1016/j.talanta.2019.02.021
6. Xu, X.; Bai, Z.; Wang, T. Portable device for on-site detection of ammonia nitrogen. Information Processing in Agriculture **2022**. DOI: 10.1016/j.inpa.2022.07.003.
7. Nishihara, H.; Toda, Y.; Kuramoto, T.; Kamohara, K.; Goto, A.; Hoshino, K.; Okada, S.; Kuraku, S.; Okabe, M.; Ishimaru, Y. A vertebrate-wide catalogue of T1R receptors reveals diversity in taste perception.

Nat Ecol Evol **2024**, *8* (1), 111-120. DOI: 10.1038/s41559-023-02258-8

8. Eggers, S.; Acree, T.; Shallenberger, R. Sweetness chemoreception theory and sweetness transduction. Food Chem **2000**, *68* (1), 45-49.
9. Mafi, A.; Kim, S.-K.; Chou, K. C.; Güthrie, B.; Goddard, W. A. Predicted Structure of Fully Activated Tas1R3/1R3' Homodimer Bound to G Protein and Natural Sugars: Structural Insights into G Protein Activation by a Class C Sweet Taste Homodimer with Natural Sugars. J Am Chem Soc **2021**, *143* (40), 16824-16838. DOI: 10.1021/jacs.1c08839.
10. Montmayeur, J. P.; Liberles, S. D.; Matsunami, H.; Buck, L. B. A candidate taste receptor gene near a sweet taste locus. Nat Neurosci **2001**, *4* (5), 492-498. DOI: 10.1038/87440.
11. Yang, J.; Guo, J.; Mai, R.; Dong, H.; Cui, C.; Zeng, X.; Bai, W. Comparing the difference in enhancement of kokumi-tasting γ-glutamyl peptides on basic taste via molecular modeling approaches and sensory evaluation. Food Sci Hum Well **2022**, *11* (6), 1573-1579.
12. Zheng, H.; Xu, X.; Fang, Y.; Sun, R.; Liu, B. The Molecular Theory of Sweet Taste: Revisit, Update, and Beyond. J Med Chem **2024**, *67* (5), 3232-3243. DOI: 10.1021/acs.jmedchem.3c02055.
13. Kalambate, P. K.; Rao, Z.; Dhanjai; Wu, J.; Shen, Y.; Boddula, R.; Huang, Y. Electrochemical (bio) sensors go green. Biosens Bioelectron **2020**, *163*, 112270. DOI: 10.1016/j.bios.2020.112270
14. Wongkaew, N.; Simsek, M.; Griesche, C.; Baeumner, A. J. Functional Nanomaterials and Nanostructures Enhancing Electrochemical Biosensors and Lab-on-a-Chip Performances: Recent Progress, Applications, and Future Perspective. Chemical Reviews **2018**, *119* (1), 120-194. DOI: 10.1021/acs.chemrev.8b00172.
15. Ronnie, C.; Bernardo, D.; Maria Gemel, P.; Jonah Jahara, B.; Argel, B.; Ryan Rhay, V.; Elmer, D. Screen-printed graphite electrode on polyvinyl chloride and parchment strips integrated with genetic programming for in situ nitrate sensing of aquaponic pond water. Information Processing in Agriculture **2024**, *11* (2), 187-201. DOI: 10.1016/j.inpa.2023.02.002.
16. Koo, B.-R.; Bae, J.-W.; Ahn, H.-J. Low-temperature conducting performance of transparent indium tin oxide/antimony tin oxide electrodes. Ceram Int **2017**, *43* (8), 6124-6129.
17. Darwish, N. T.; Alias, Y.; Khor, S. M. Indium tin oxide with zwitterionic interfacial design for biosensing applications in complex matrices. Appl Surf Sci **2015**, *325*, 91-99.
18. Mitsubayashi, K.; Wakabayashi, Y.; Tanimoto, S.; Murotomi, D.; Endo, T. Optical-transparent and flexible glucose sensor with ITO electrode. Biosens Bioelectron **2003**, *19* (1), 67-71. DOI: 10.1016/s0956-5663(03)00130-1
19. Wang, J.; Yu, J.; Yu, Y.; Luo, Z.; Li, G.; Lin, X. Nanoporous electrode with stable polydimethylsiloxane coating for direct electrochemical analysis of bisphenol A in complex wine media. Food Chem **2023**, *405*, 134806.
20. Xie, Z.; Lin, M.; He, X.; Dong, Y.; Chen, Y.; Li, B.; Chen, S.; Lv, G. Chemical Constitution, Pharmacological Effects and the Underlying Mechanism of Atractylenolides: A Review. Molecules **2023**, *28* (10). DOI: 10.3390/molecules28103987

21. Yang, L.; Yu, H.; Hou, A.; Man, W.; Wang, S.; Zhang, J.; Wang, X.; Zheng, S.; Jiang, H.; Kuang, H. A Review of the Ethnopharmacology, Phytochemistry, Pharmacology, Application, Quality Control, Processing, Toxicology, and Pharmacokinetics of the Dried Rhizome of Atractylodes macrocephala. Front Pharmacol **2021**, *12*, 727154. DOI: 10.3389/fphar.2021.727154
22. De Guzman, N.; Ramos Jr, M.; Balela, M. D. Improvements in the electroless deposition of Ag nanowires in hot ethylene glycol for resistive touchscreen device. Mater Res Bull **2018**, *106*, 446-454.
23. Deng, Y.; Li, J.; Qian, T.; Guan, W.; Li, Y.; Yin, X. Thermal conductivity enhancement of polyethylene glycol/expanded vermiculite shape-stabilized composite phase change materials with silver nanowire for thermal energy storage. Chem Eng J **2016**, *295*, 427-435.
24. Khodashenas, B.; Ghorbani, H. R. Synthesis of silver nanoparticles with different shapes. Arab J Chem **2019**, *12* (8), 1823-1838.
25. Zhang, Q.; Jiang, D.; Xu, C.; Ge, Y.; Liu, X.; Wei, Q.; Huang, L.; Ren, X.; Wang, C.; Wang, Y. Wearable electrochemical biosensor based on molecularly imprinted Ag nanowires for noninvasive monitoring lactate in human sweat. Sens Actuators B Chem **2020**, *320*, 128325.
26. Zhu, Y.; Wang, P.; Ma, Q.; Zhang, Z. The PVDF-HFP/Ag NWs-based wide electrochemical stability window ECL system for miRNA 21 detection in gastric cancer ascites. Chem Eng J **2023**, *469*, 144025.
27. Nantaphol, S.; Chailapakul, O.; Siangproh, W. Sensitive and selective electrochemical sensor using silver nanoparticles modified glassy carbon electrode for determination of cholesterol in bovine serum. Sensor Actuat B-Chem **2015**, *207*, 193-198. DOI: 10.1016/j.snb.2014.10.041.
28. Qin, X.; Wang, H. C.; Miao, Z. Y.; Wang, X. S.; Fang, Y. X.; Chen, Q.; Shao, X. G. Synthesis of silver nanowires and their applications in the electrochemical detection of halide. Talanta **2011**, *84* (3), 673-678. DOI: 10.1016/j.talanta.2011.01.064.
29. Gogurla, N.; Roy, B.; Park, J.-Y.; Kim, S. Skin-contact actuated single-electrode protein triboelectric nanogenerator and strain sensor for biomechanical energy harvesting and motion sensing. Nano Energy **2019**, *62*, 674-681.

Figures

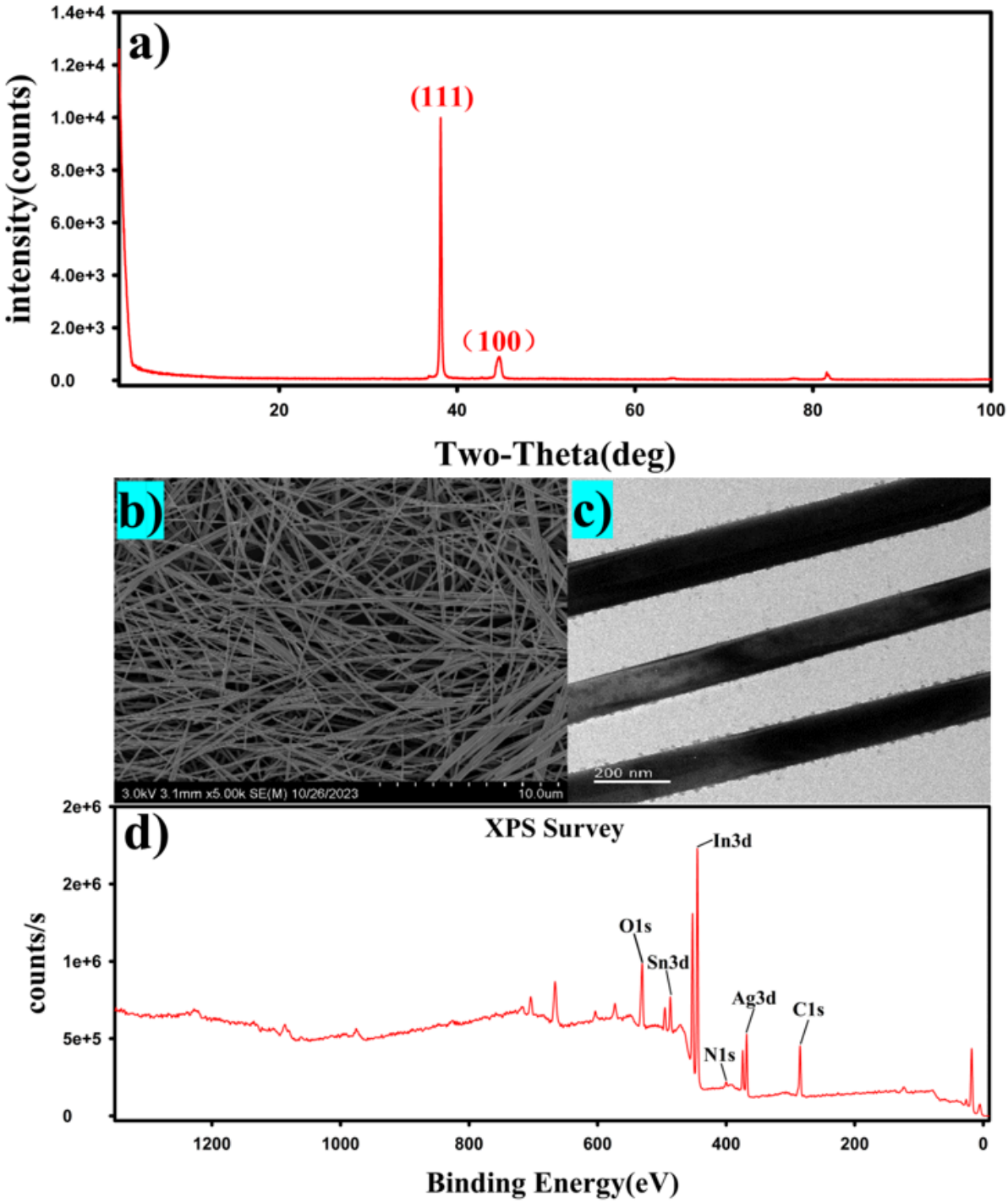


Figure 1

Structural and morphological characterization of the synthesized AgNWs. a) XRD characterisation of AgNWs; b) SEM characterisation of AgNWs; c) TEM characterisation of AgNWs; d) XPS characterisation of AgNWs.

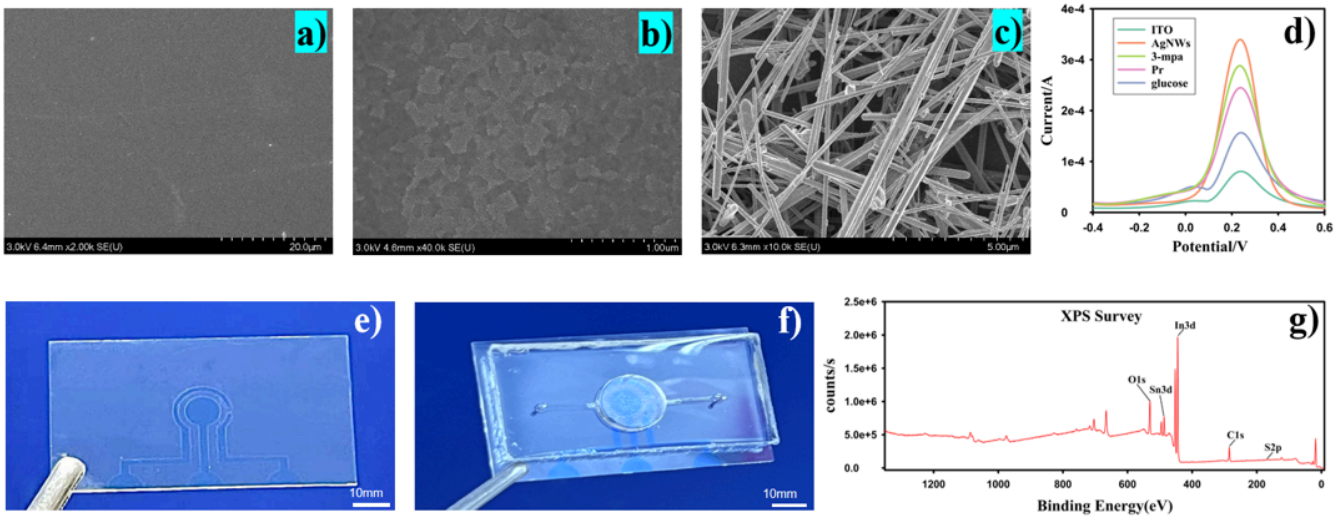


Figure 2

SEM, DPV and XPS tracking of ITO/AgNWs sensor build-up. a) SEM characterisation of bare glass sheet; b) SEM characterisation of glass sheet modified with ITO; c) SEM characterisation of ITO glass after modification with AgNWs; d) Differential Pulse Voltammetry characterization of layer-by-layer modification process; e) ITO electrode; f) Microfluidic chip for electrodes; g) XPS characterisation of ITO@AgNWs.

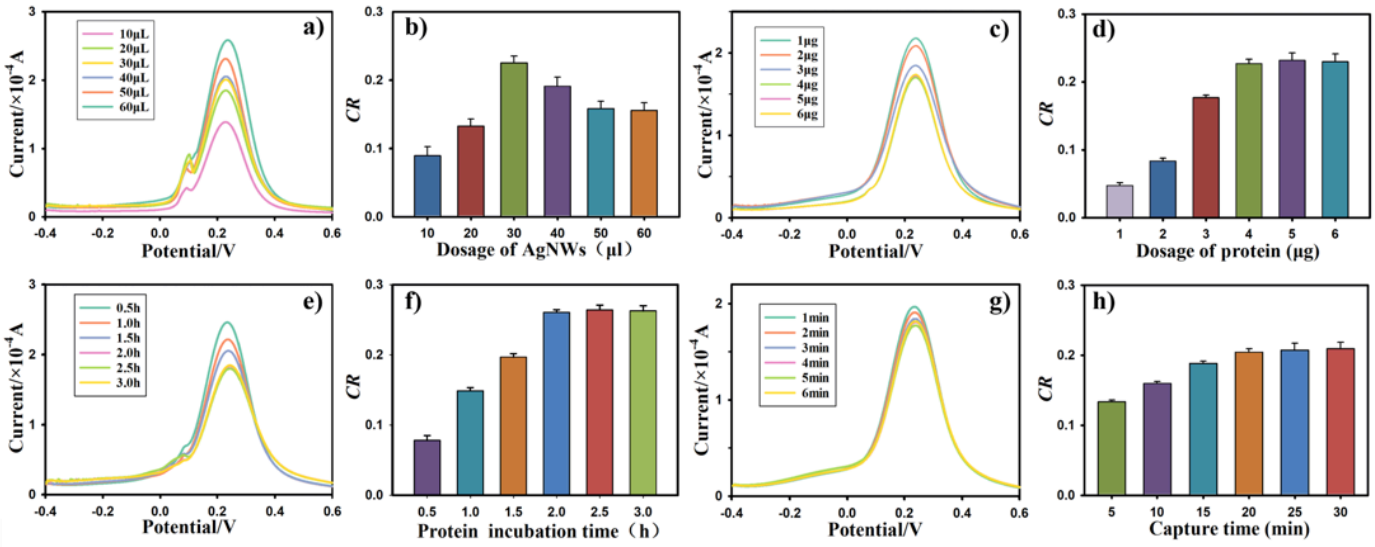


Figure 3

Optimisation of experimental parameters. a) DPV signal response results of AgNWs dosages; b) Relative change in biosensor current with different AgNWs dosages; c) DPV signal response results of different protein dosages; d) Relative change in biosensor current with different protein dosages; e) DPV signal response results of different protein modification times; f) Relative change in biosensor current with

different protein modification times; g) DPV signal response results of different capture times; h) Relative change of biosensor current at different capture times(N=3).

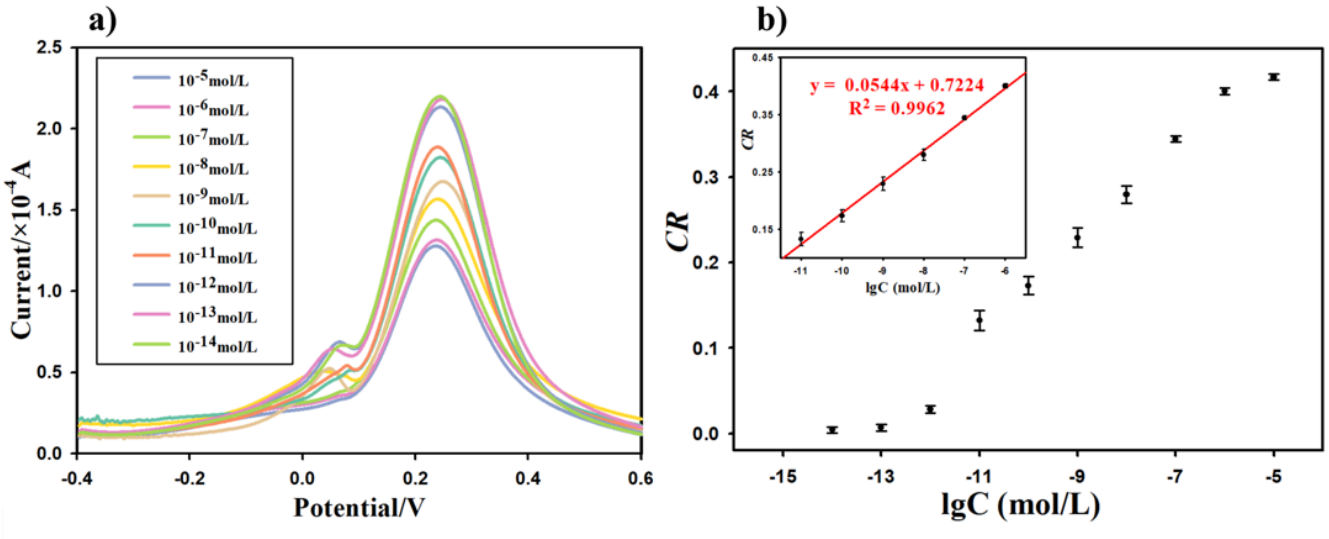


Figure 4

Biosensor performance analysis. a) Differential pulse voltammetric characteristic curves at different concentration solutions; b) Linearity of logarithm of concentration of T1R2@AgNWS/ITO biosensor ATR-I versus relative value of current change.

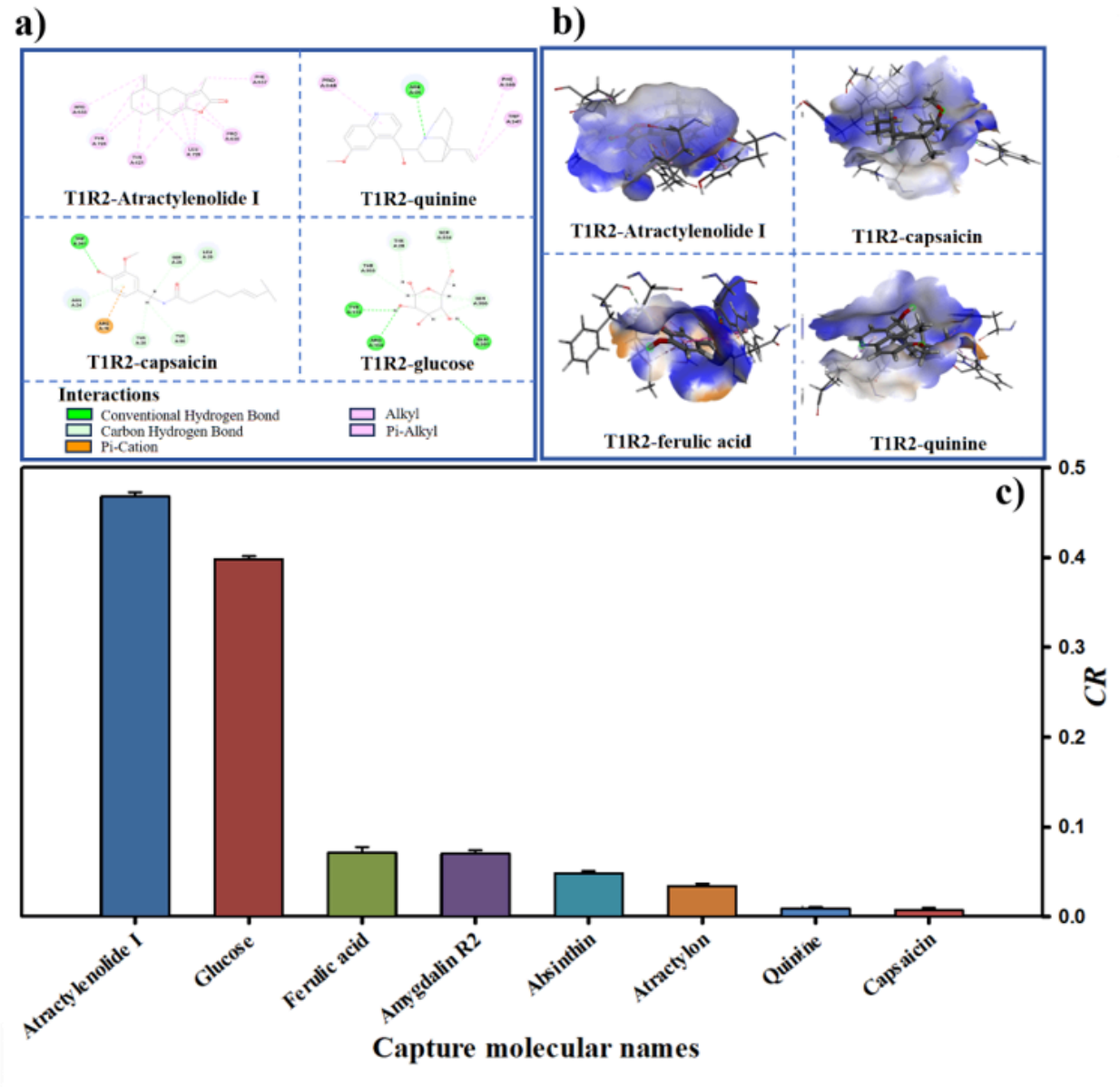


Figure 5

Molecular interaction, specificity, and sweetness-related evaluation of ATR-I. a) Schematic of 2D plane of interaction of different ligand molecules with T1R2 protein; b) Schematic of 3D plane of interaction of different ligand molecules with T1R2 protein; c) Relative variation of biosensor currents for different ligand molecules (N=3).

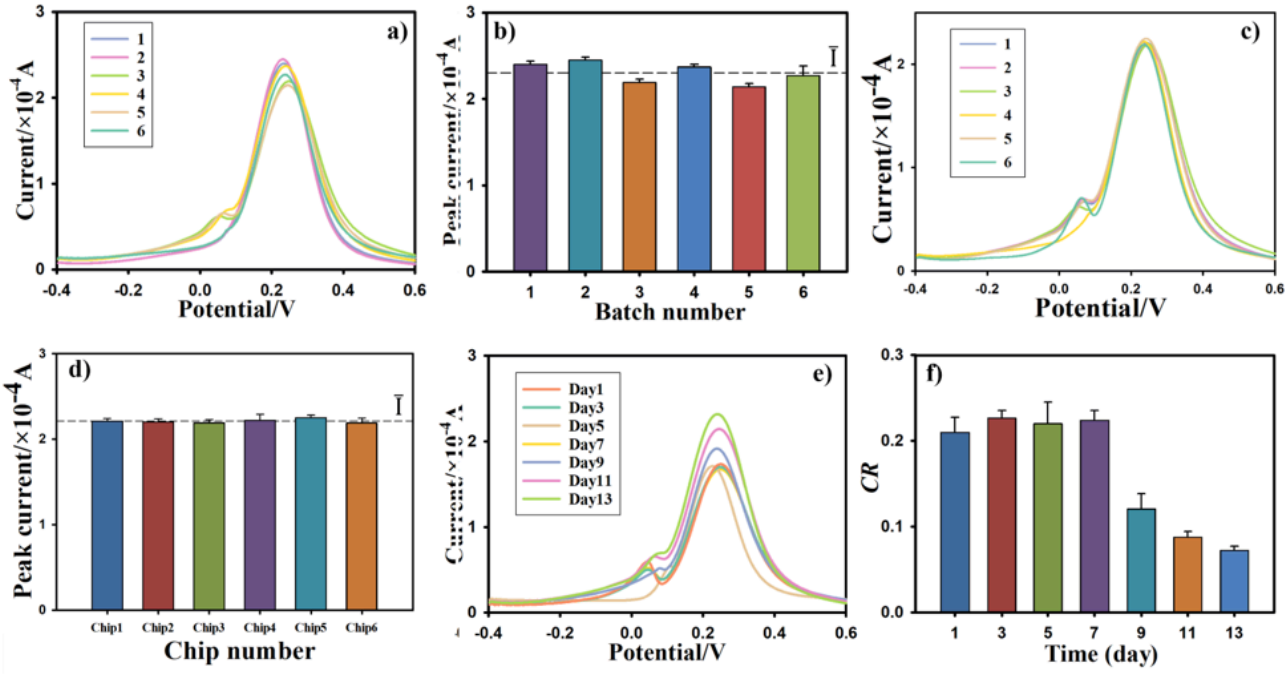


Figure 6

Evaluation of reproducibility and long-term storage stability of the biosensor. (a) DPV curves and (b) corresponding peak-current signals of six independently-fabricated sensor batches for inter-batch reproducibility; (c) DPV curves and (d) corresponding peak-current signals of six parallel electrodes from a single batch for intra-batch reproducibility; (e) DPV responses and (f) relative current-change ratios of the biosensor stored over 13 days at 4 °C, measured using 1 nM ATR-I as the target analyte(N=3).

Supplementary Files

This is a list of supplementary files associated with this preprint. Click to download.

- supplementary.docx
- GraphicalAbstract.png